SONIC BOOM PREDICTIONS USING A MODIFIED EULER CODE+

M.J.Siclari
Grumman Corporate Research Center
Bethpage, New York

First Annual
HIGH-SPEED RESEARCH WORKSHOP
May 14-16,1991
Williamsburg, Virginia

+ This work was sponsored by NASA Langley Research Center, Advanced Vehicle Division, Dr. Christine Darden

INTRODUCTION

The environmental impact of a next generation fleet of high-speed civil transports (HSCT) is a great concern in the evaluation of the commercial development of such a transport. One of the potential environmental impacts of a high speed civilian transport is the sonic boom generated by the aircraft and its effects on the population, wildlife, and structures in the vicinity of its flight path. If an HSCT aircraft is restricted from flying overland routes due to excessive booms, the commercial feasibility of such a venture may be questionable.

NASA has taken the lead in evaluating and resolving the issues surrounding the development of a high speed civilian transport through it High-Speed Research Program (HSRP).

The present paper discusses the usage of a Computational Fluid Dynamics (CFD) nonlinear code in predicting the pressure signature and ultimately the sonic boom generated by a high speed civilian transport.

NASA has designed, built, and wind tunnel tested two low boom configurations for flight at Mach 2 and Mach 3 (see Ref. 1). Experimental data was taken at several distances from these models up to a body length from the axis of the aircraft. The near field experimental data serves as a test bed for computational fluid dynamic codes in evaluating their accuracy and reliability for predicting the behavior of future HSCT designs.

Sonic boom prediction methodology exists which is based on modified linear theory. These methods can be used reliably if near field signatures are available at distances from the aircraft where nonlinear and three dimensional effects have diminished in importance. Up to the present time, the only reliable method to obtain this data was via the wind tunnel with costly model construction and testing.

It is the intent of the present paper to apply a modified three dimensional Euler code to predict the near field signatures of the two low boom configurations recently tested by NASA.

APPROACH

In order to compute the supersonic flow field about a configuration, a three dimensional Euler code called MIM3D (Multigrid-Implicit-Marching) was modified to accommodate the unique prediction of sonic boom signatures below and aft of an aircraft configuration. The numerical scheme is based on a Jameson type finite volume vertex Runge-Kutta scheme (Ref.2). Further documentation of the present method as applied to high speed flows can be found in Refs. 3 and 4.

The three dimensional unsteady Euler equations are solved using an implicit marching technique. Stability and smooth shocks are maintained with the addition of second and fourth order dissipation. The steady state solution at each marching plane is obtained using an explicit multi-stage Runge-Kutta time integration scheme with local time stepping and implicit residual smoothing to accelerate convergence. To further accelerate convergence to a steady state solution in each marching plane, a multigrid scheme can also be applied in the crossflow plane.

The solution is started at the apex of the configuration by assuming a small conical nose cap based on the geometry of the configuration at the first step. The unique aspects of this technique is that it is very fast and requires very little memory for large grids.

The sonic boom version of this code called MIM3DSB has been modified to retain accuracy for sonic boom computations. Unlike aerodynamic computations, where only accurate surface data needs to be predicted, sonic boom computations require accuracy in the field below and aft of the aircraft. For example, to predict a pressure signature just one body length below an HSCT flying at Mach 3, the computation must be carried out with sufficient accuracy to 3 body lengths aft of the end of the configuration. Since the same number of grid points normal to the body are available, a loss in resolution occurs as the computation proceeds aft of the end of the vehicle.

Some of the key modifications incorporated into the present method to retain accuracy are as follows:

- adaptive outer grid boundary that automatically senses the bow shock wave and adapts the grid

- downstream boundary that corresponds to the freestream Mach cone

- multiblock grid that allows for a switch from a wing-body type grid with a slit for wake matching to a simple polar grid aft of the configuration

- sonic boom pressure signature output at user specified distances below the aircraft. These signatures can then be extrapolated to the ground using sonic boom extrapolation methods.

The present sonic boom Euler code has been applied to axisymmetric projectiles and wing-body configurations in Ref. 5.

Figure 1 shows a side view of a typical grid topology used in the present Euler code for the Mach 3 low boom configuration. The aircraft is extended with a sting. In this case, the sting represents the actual sting used to support the model in the wind tunnel. The sting then terminates in a Mach cone surface where freestream boundary conditions are applied. The grid is then restricted to lie between the outer boundary just outside the bow wave and a downstream Mach surface. The outer boundary is progressively adapted to the shape of the bow wave by the computation. Essentially, the outer boundary is part of the solution. To compute a pressure signature at just one body length normal to the axis of the Mach 3 aircraft, the computation must be carried out 3 to 4 body lengths aft of the aircraft. As illustrated by Figure 1, if the grid topology was extended to the axis of the aircraft, a loss of accuracy of the solution would occur due to the increase in distance from the aircraft axis to the outer grid boundary as the computation proceeded downstream.

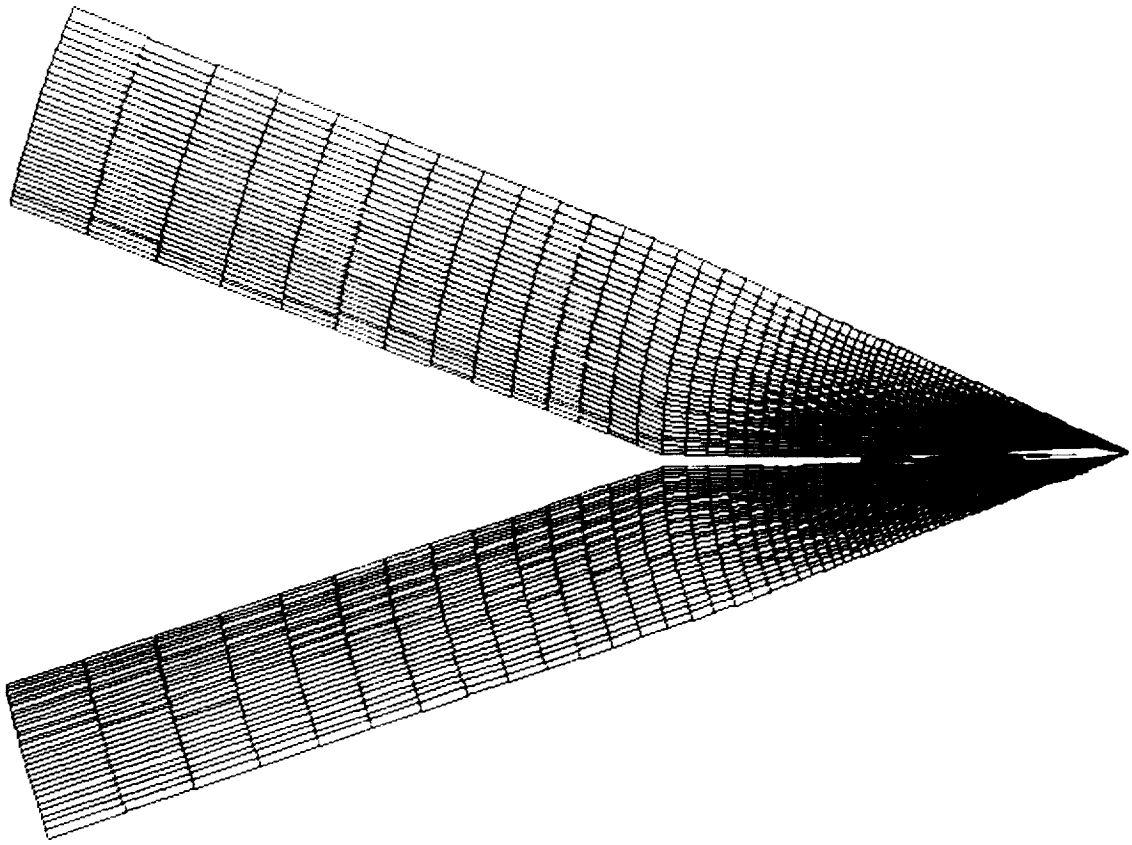

Figure 1 Side View of Grid Topology Used For Sonic Boom Computations

Figure 2 shows the overall grid topology for the Mach 3 low bow configuration. A typical stacked crossflow plane grid topology is used over the aircraft. At the end of the wing, the grid is switched to a new block with a polar grid containing the sting. Hence, the computation is performed using two grid blocks. One contains the aircraft, and the second block, the sting and Mach surface. The furthest distance downstream at which the computation remains valid is determined by the length of the sting extension. This occurs because the sting effects the strength of the tail shock. If the sting is too short, the Mach surface, where artificial freestream boundary conditions are imposed, will effect the formation of the tail shock. Typically, the length of the sting varied by a half to one aircraft length. This allowed for computations of pressure signatures from one to three body lengths normal to the aircraft axis. The length of the sting also effects accuracy for a given grid resolution. As the sting is made longer, and distance between outer boundary and Mach surface increases causing a loss in accuracy given the same number of mesh points.

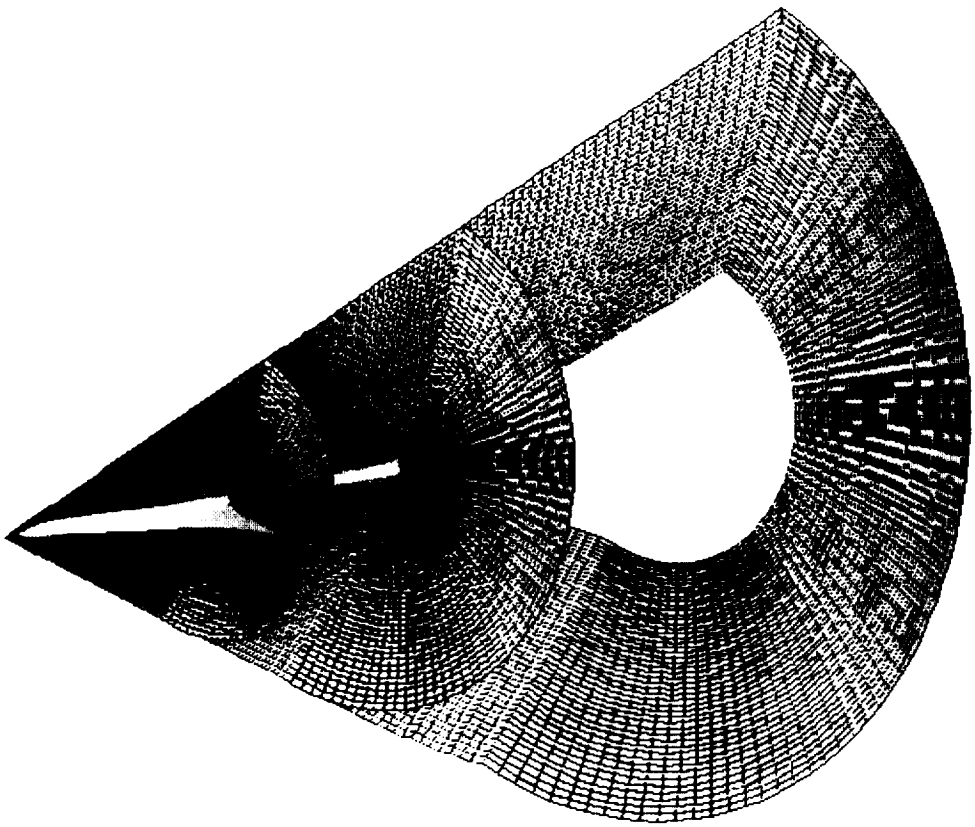

Figure 2 Three Dimensional View of Sonic Boom Grid Topology

Figure 3 shows the geometry and computed aft pressure contours at $M_\infty = 3.0$, $\alpha = 1.97°$ for NASA's Mach 3 low boom configuration. The Mach 3 model has a needle nose and a highly swept wing which cranks to a supersonic leading edge. The cranked wing generates a strong shock as indicated by the isobars. The fuselage is also fitted to a sting where a shock at the attachment point to the sting is also indicated by the isobars. As mentioned earlier, the solution is carried out on two mesh blocks. The resolution of the mesh block containing the aircraft was (89 x 91) in the crossflow plane with 106 marching steps. The resolution of the second block was (95 x 95) by 127 marching steps for a computation carried out to three body lengths normal to the aircraft axis or 12 body lengths downstream of the aircraft. The second block does not use a fixed axial step size but a stretching function that gradually increases the step size. The axial step size far downstream can be as much as one-half the aircraft body length. Hence, approximately 850,000 points were used to compute the flow in the vicinity of the aircraft and approximately 1.1 million points were used to compute the flow to 15 body lengths downstream of the aircraft.

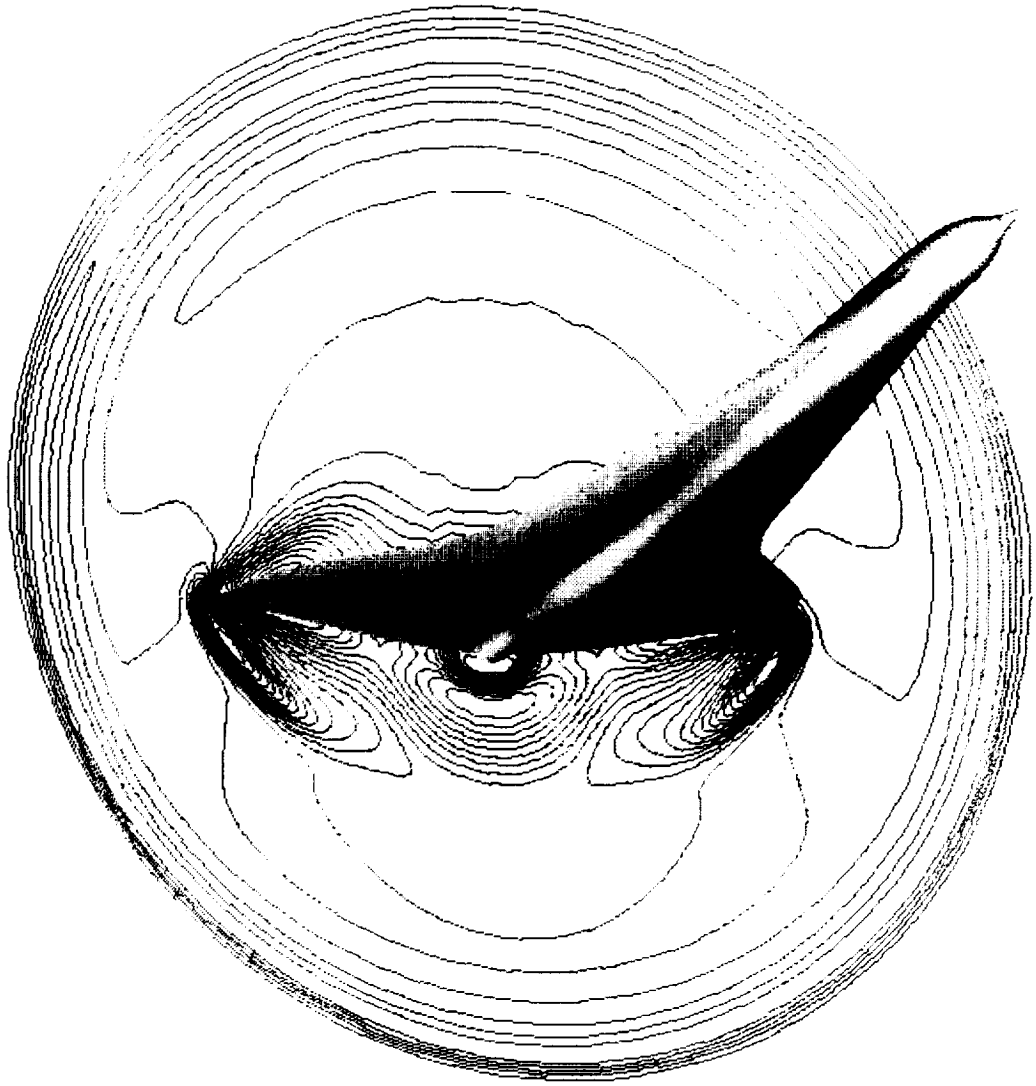

Figure 3 NASA's Mach 3 Low Boom Configuration

Figure 4 shows the near field computed pressure contours for the Mach 3 configuration at M_∞ = 3.0, α = 1.97°. The symmetry plane and back plane contours are both illustrated. The bow shock is clearly evident. The contours are relatively clean in the symmetry plane up to the aft end of the aircraft. In this region, several shocks begin to appear. The sting attachment shock and a strong shock around the leading edge of the wing due to the wing crank.

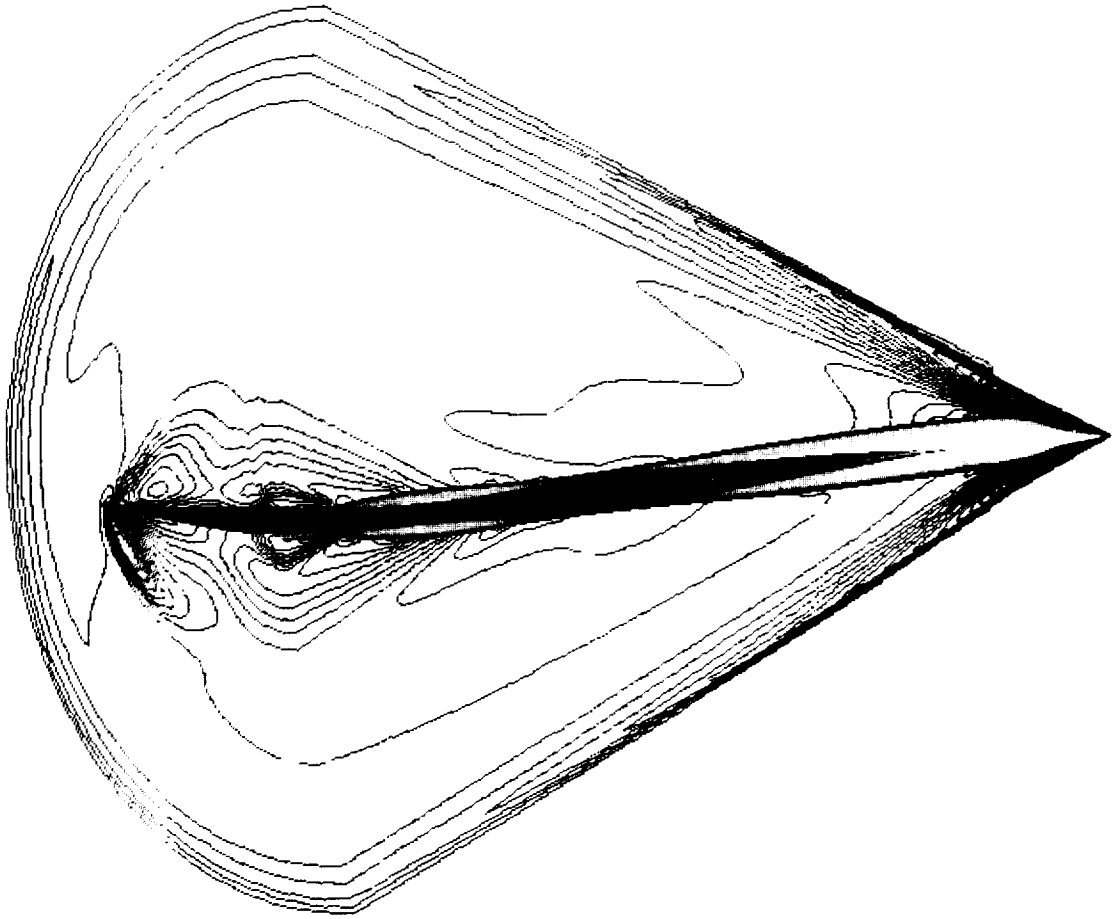

Figure 4 Near Field Pressure Contours for the Mach 3 Configuration

Figure 5 shows the computed symmetry plane pressure contours for the Mach 3 configuration at $M_\infty = 3.0$, $\alpha = 1.97°$. In this figure, the sting is shown which is almost an aircraft length in size. Towards the aft end of the aircraft, the contour of the fuselage produces a large expansion terminated in a shock at the sting attachment point. A wing trailing edge shock may also occur but is not evident in the isobars.

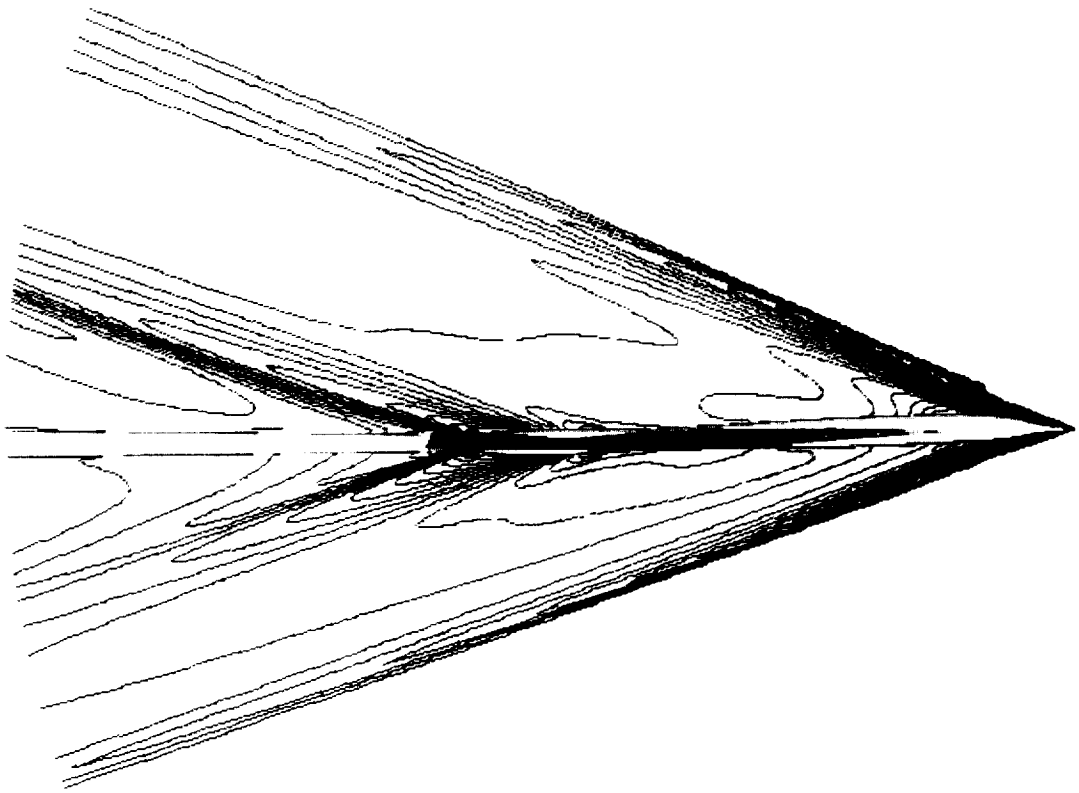

Figure 5 Symmetry Plane Pressure Contours for the Mach 3 Configuration

Figure 6 dramatically displays the sonic boom computation and the complexity of the flow field downstream of the aircraft. The computed isobars are shown in a plane at the end of the sting. In the leeward part of this plane, a strong shock is shown. This is probably the coalescence of the wing trailing edge shock and sting attachment shock. On the windward side, the situation is less clear and clearly more complex. A strong shock occurs due to the wing crank and expansion due to the wing tip. It is interesting to note that the circular isobars just to the right and left of the sting are vortices generated by the wing tips.

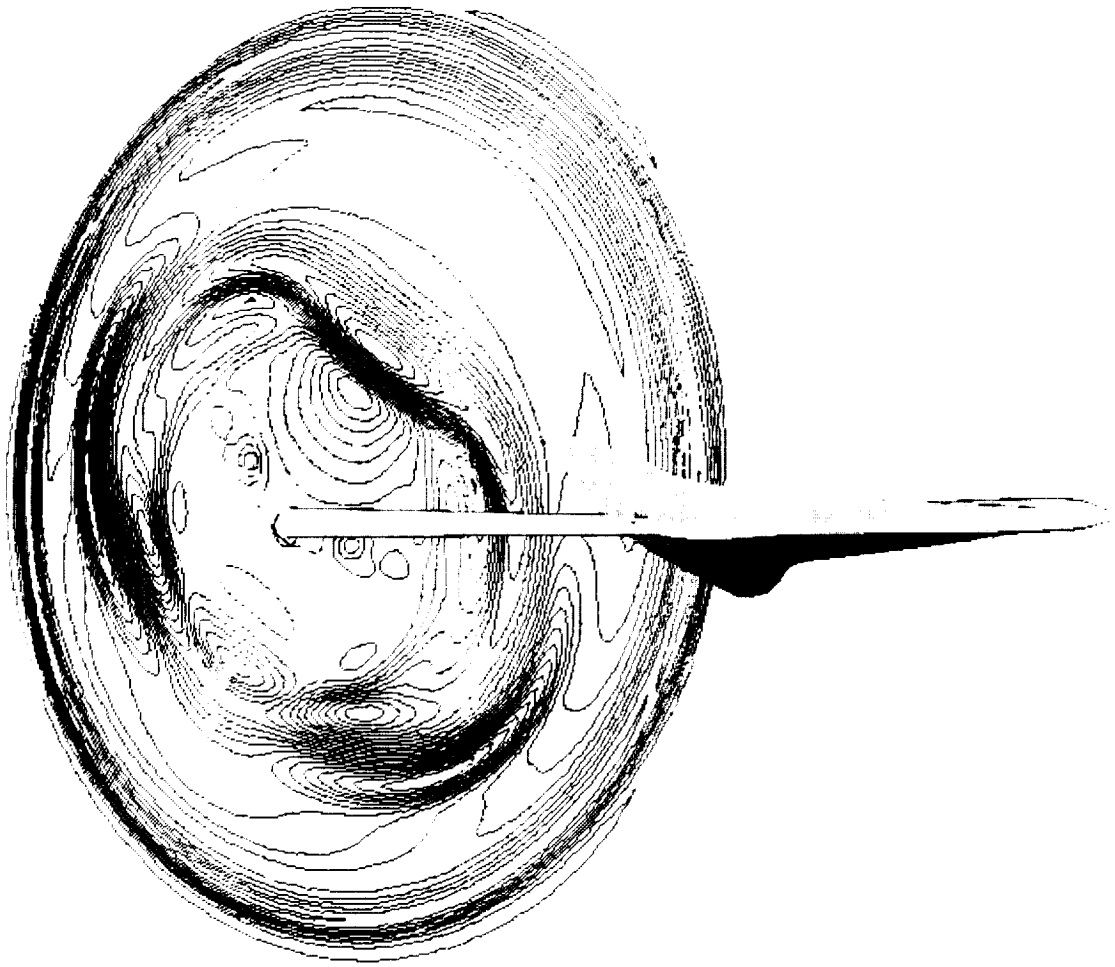

Figure 6 Near-Field Downstream Pressure Pattern of the Mach 3 Configuration

Figure 7 further illustrates the sonic boom computation for the Mach 3 configuration flying at $M_\infty = 3.0$, $\alpha = 1.97°$. In this figure, three downstream planes are shown with their computed isobar pressure patterns.

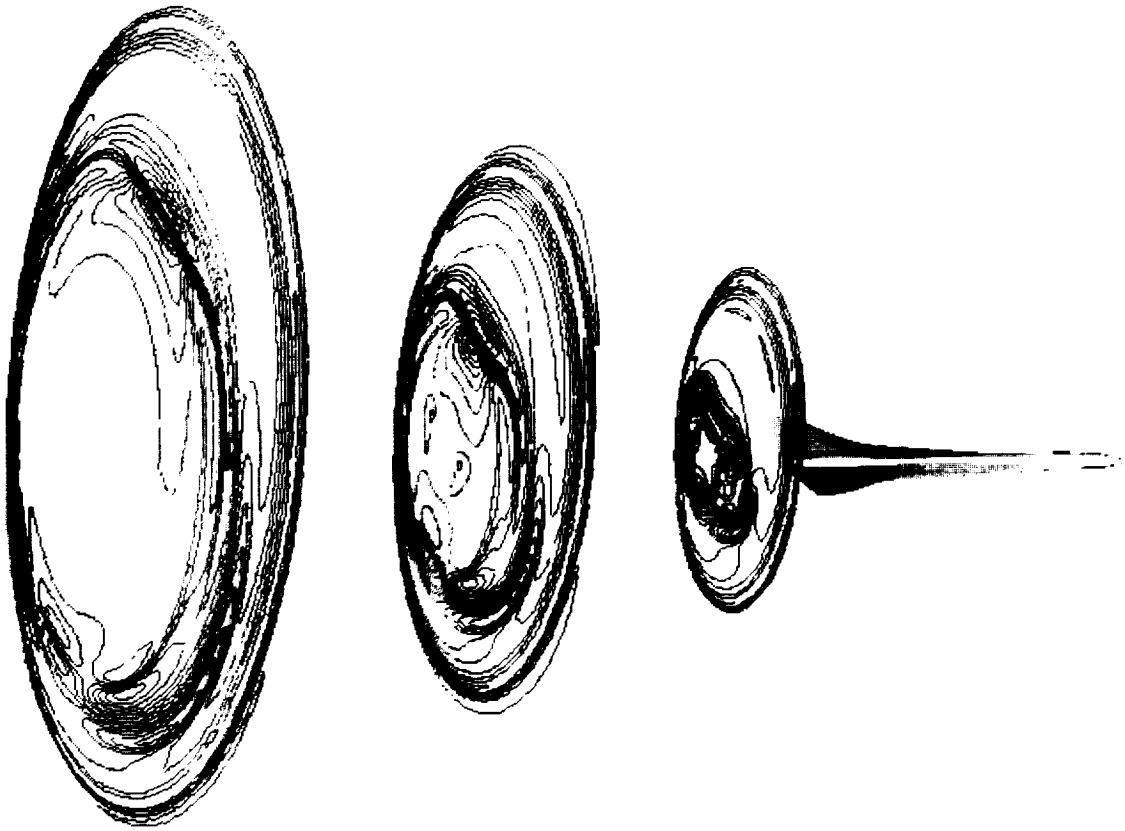

Figure 7 Propagation of Midfield Downstream Pressure Patterns for the Mach 3 Configuration

Figure 8 shows the geometry and computed back plane isobars at $M_\infty = 2.0$, $\alpha = 0.67°$ for the NASA Mach 2 low boom configuration. This configuration has a flat platypus nose which is blunt in planeform. Several shocks are illustrated in the back plane isobar pattern including wing trailing edge and wing crank shocks. The computation was performed on a 89 x 91 crossflow plane grid by 104 steps for the aircraft. The resolution of the second grid block was 95 x 95 with 116 marching steps to carry the computation out to 10 body lengths downstream of the aircraft. Hence, both the Mach 2 and Mach 3 configurations required about 2 million points to achieve signatures three body lengths normal to the aircraft axis.

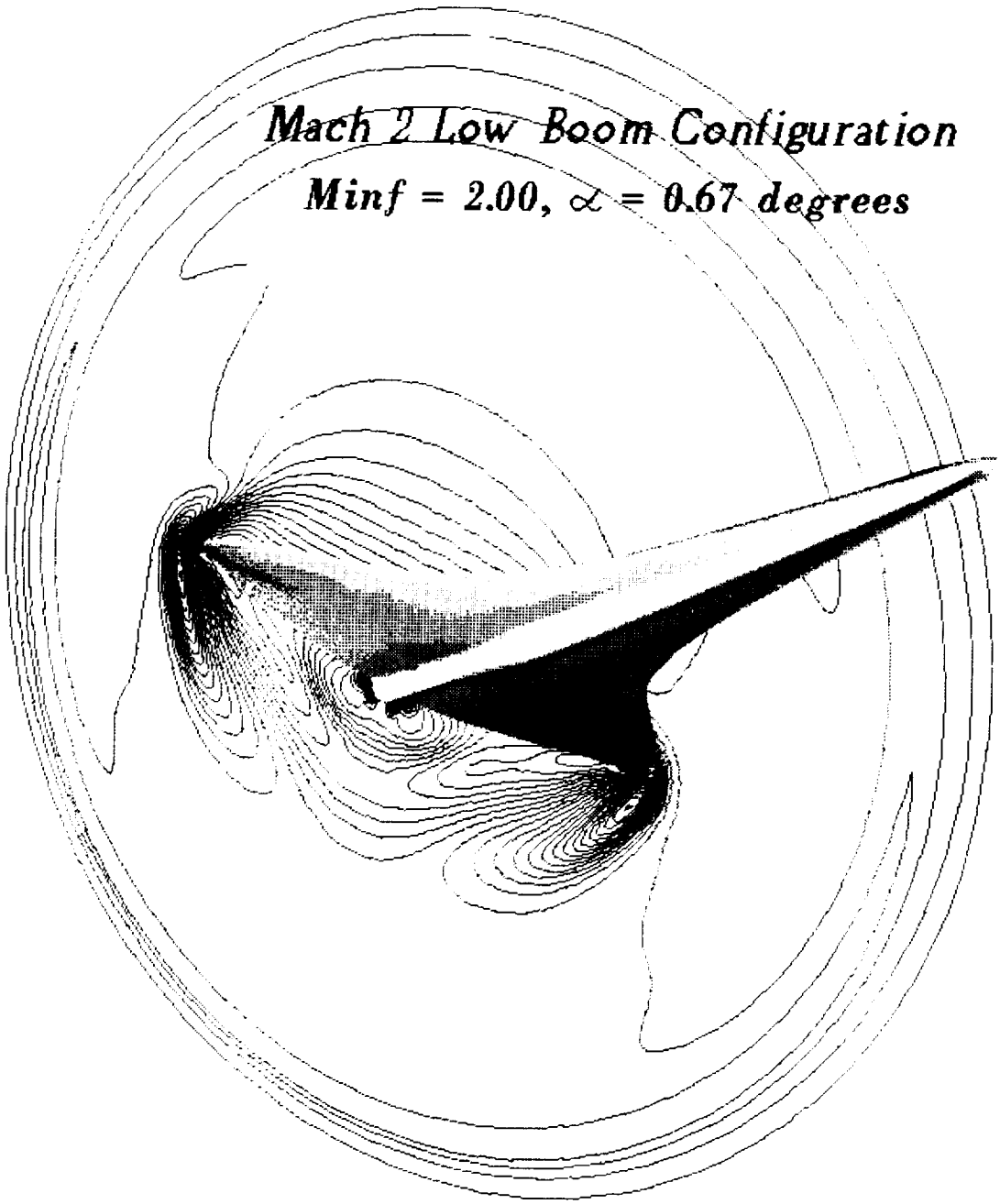

Figure 8 NASA's Mach 2 Low Boom Configuration

Figure 9 shows the computed isobars for the Mach 2 configuration at $M_\infty = 2.0$, $\alpha = 0.67°$. The symmetry plane and back crossflow plane pressure patterns are illustrated. The strong attached shock generated by the supersonic leading edge crank of the wing is clearly shown. The leeward isobars in the back plane clearly shows the trailing edge shock of the wing.

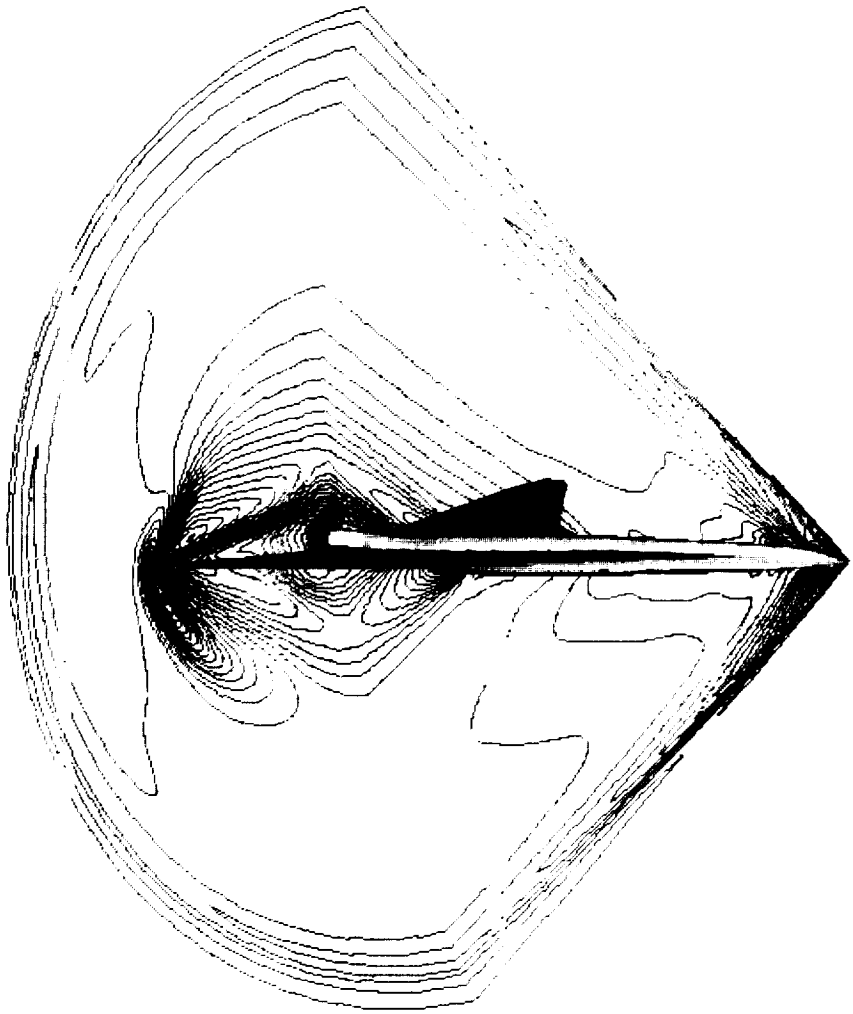

Figure 9 Near Field Pressure Contours for the Mach 2 Configuration

Figure 10 shows the symmetry plane contours for the Mach 2 configuration extending about one aircraft length behind. A strong trailing edge shock is shown in the leeward plane. There are possibly two shocks shown in the windward plane, neither of which extend very far into the field below the aircraft in comparison to the leeward plane.

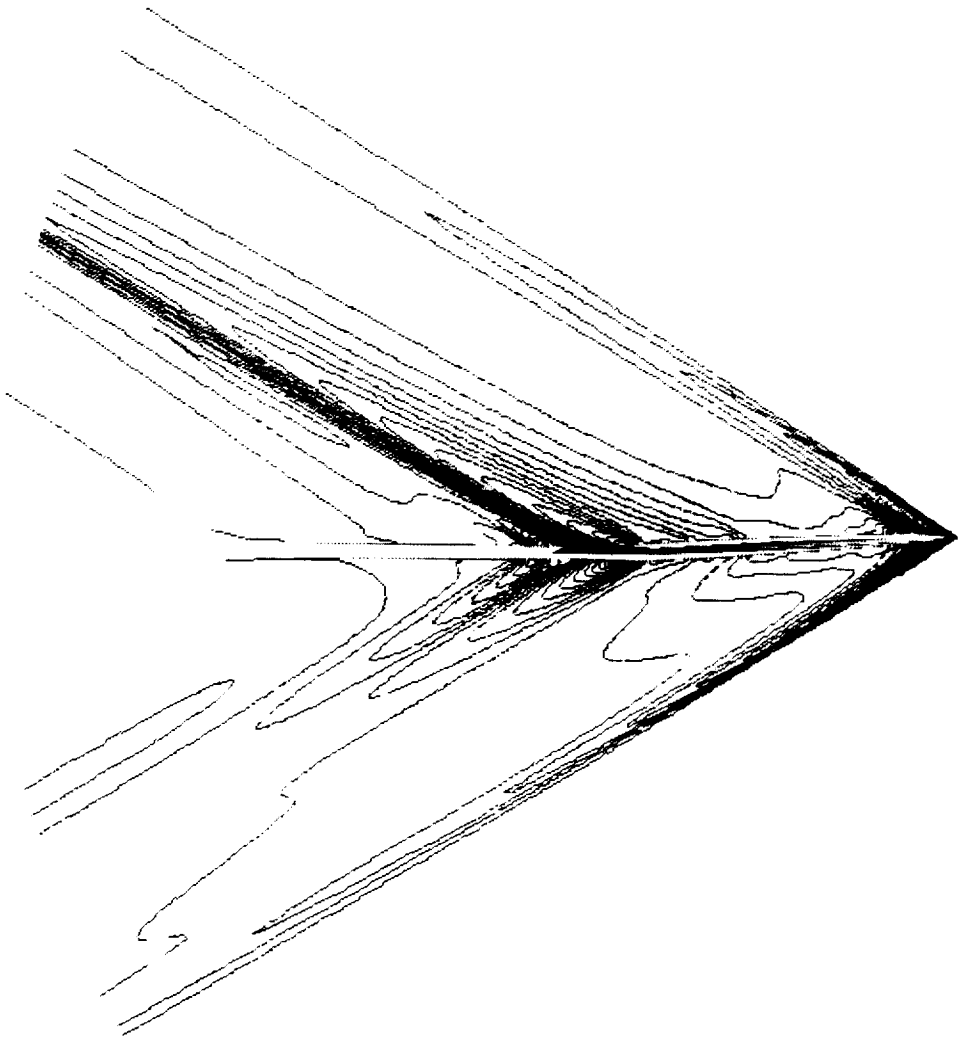

Figure 10 Symmetry Plane Pressure Contours for the Mach 2 Configuration

Figure 11 shows the computed isobars in two planes aft of the Mach 2 configuration indicating the complex flow pattern generated by the aircraft. The leeward trailing edge shock is shown and the wing crank leading edge shock. The wing crank shock does not appear to extend to the windward symmetry plane.

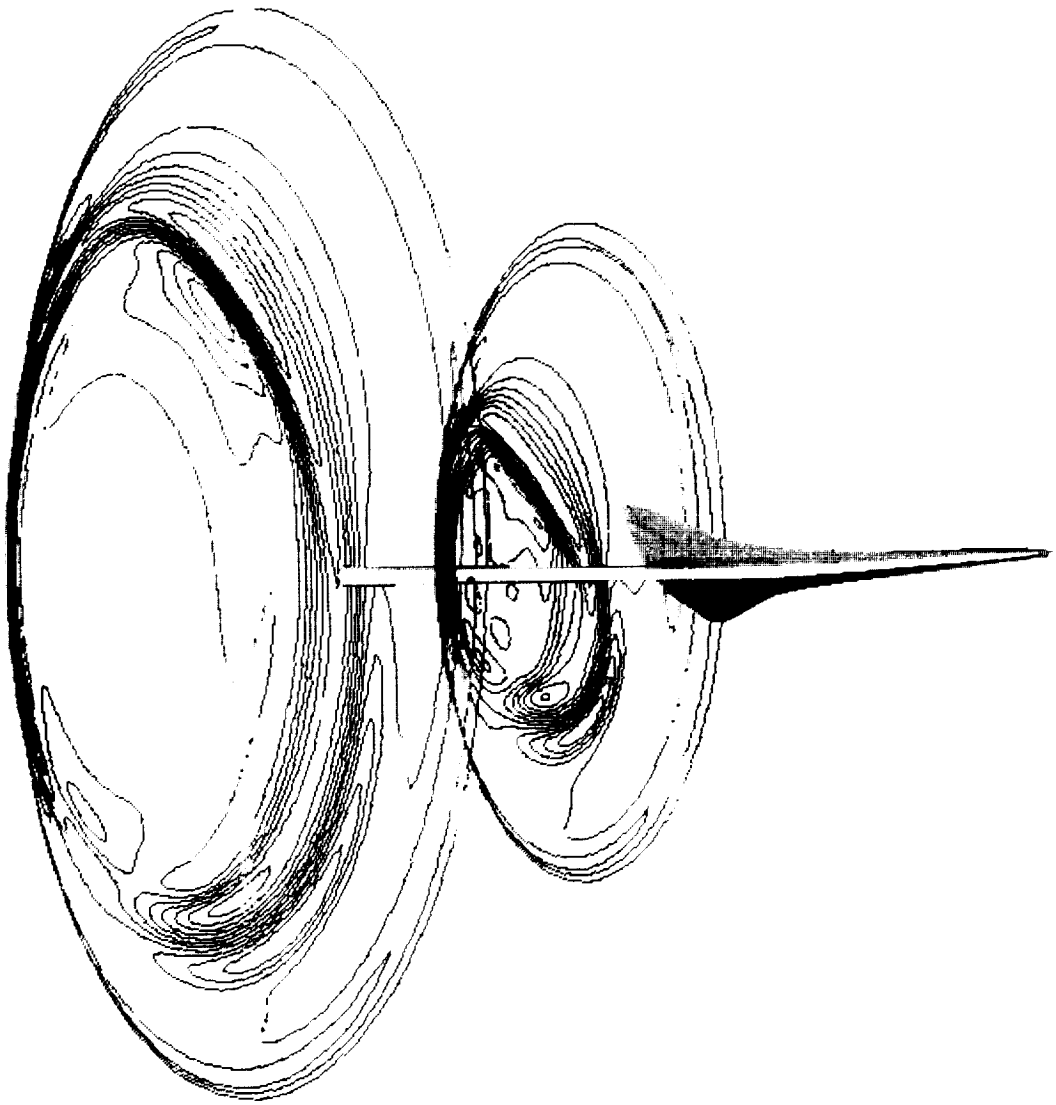

Figure 11 Propagation of Downstream Pressure Pattern of Mach 2 Configuration

Two sets of computations for each configuration were carried out with the same grid density except with different length stings. One set of computations had a sting one half of the aircraft length and the other with .8 of an aircraft length. The longer sting reduced the resolution somewhat because it increases the spatial distance between the outer boundary and downstream Mach cone boundary given a fixed number of grid points. The longer sting allowed for obtaining solutions for pressure signatures up to three body lengths normal to the aircraft axis. The shorter sting gave valid solutions for one body length. Figure 12a shows the computed pressure signatures very close to the body at $h/\ell = 0.17$ and 0.50 where the nondimensionalizing length ℓ was taken to be 300 feet for both Mach 2 and Mach 3 configurations. At $h/\ell = 0.17$, a strong bow shock overpressure occurs followed by a relatively flat signature until the back end of the aircraft. An expansion occurs due to the shape of the fuselage followed by a single shock due to the sting attachment or wing trailing edge or both. The signature decays very rapidly to $h/\ell = 0.50$. Figure 12b shows the effect of the sting length on the computed pressure signatures below the two configurations at one body length. The pressures are plotted versus full scale coordinates in feet. In both cases the first half of the signature agrees well. The strength of the shock just prior to the rear expansion is slightly stronger in both cases for the shorter sting with effectively higher resolution. It is interesting to note that the length of the signature up to the expansion is about one body length. The overall length of the signatures is about 1.5 to 2 aircraft lengths. The expansion and recompression occurs aft of the configuration. In the Mach 3 signature, the Mach cone boundary is beginning to interfere with the solution as indicated by the very rapid recompression of the tail shock.

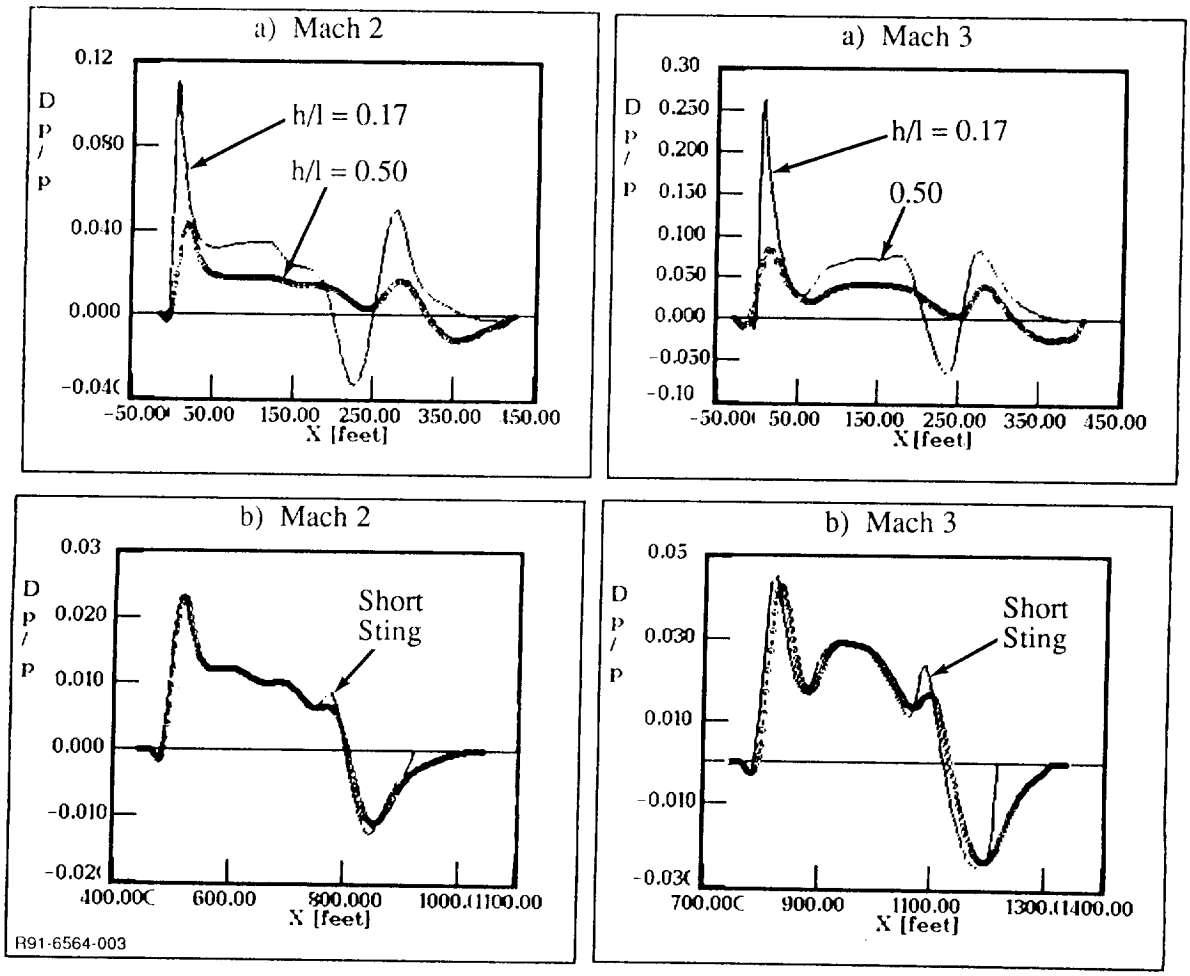

Figure 12 Computed Near Field Pressure Signatures for the Mach 2 and Mach 3 Configurations

Figure 13 shows the computed pressure signatures compared to recent wind tunnel model data (see Ref. 1) for both the Mach 2 and Mach 3 configurations. Both models were 1/300 scale or about 12 inches in length. The wind tunnel model data was converted to full scale in feet to compare to the computations. The wind tunnel data was taken at two different distances below the aircraft for each configuration. For both configurations, good correlation with the data is shown for both distances for the forward half of the signature. At $h/\ell = 0.5$, the Mach 2 data shows a series of shocks and expansions in the last half of the signature. The computation shows a single shock and expansion. At $h/\ell = 1.0$, slightly better correlation is achieved. The data stills show a series of shocks and expansions with a final very large expansion twice that of the computation. Virtually the same type of correlation is shown for the Mach 3 configuration. At the present time, the origin of these multiple shocks and large expansion shown on the latter half of the signature is unknown.

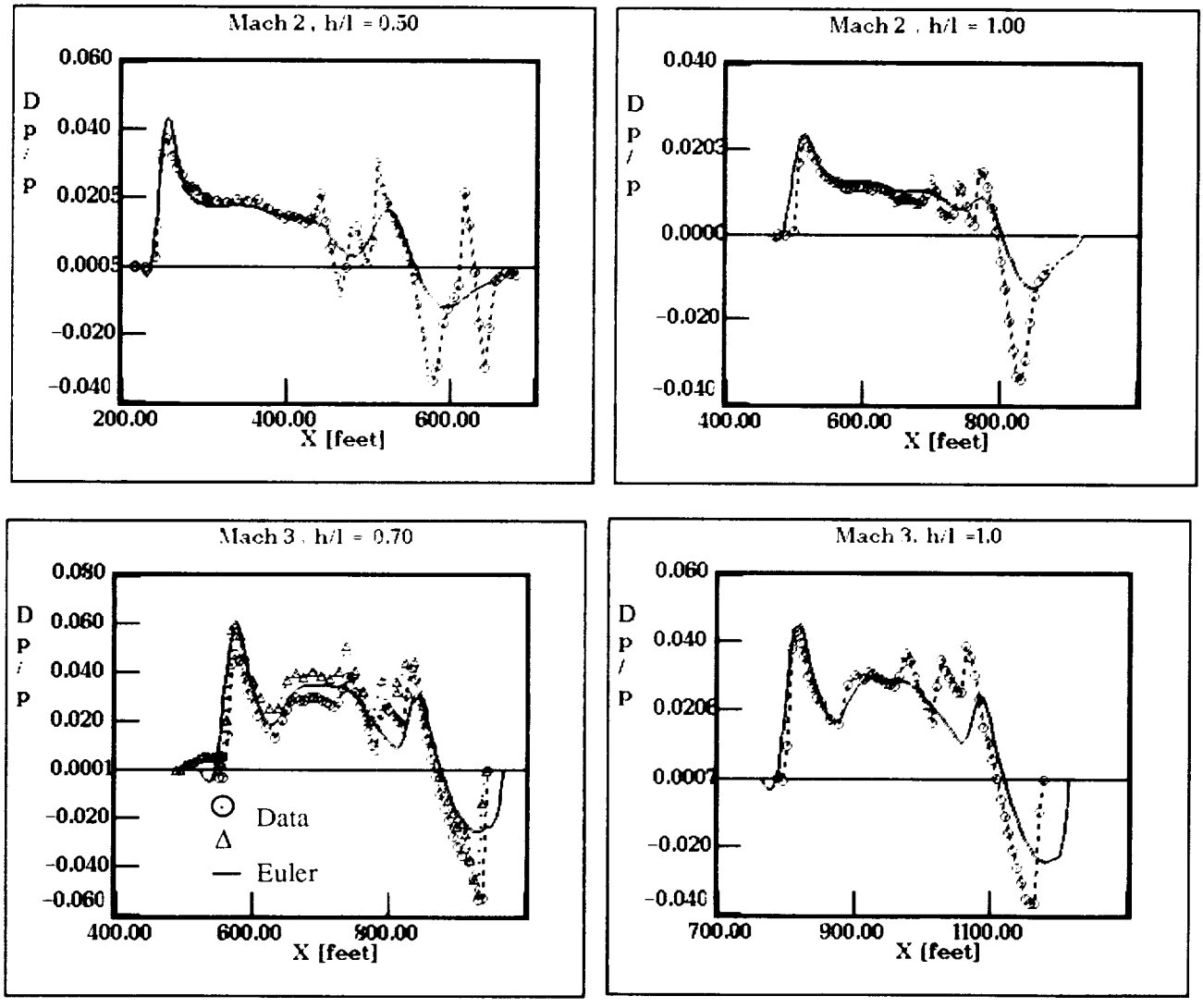

Figure 13 Comparison of Computed Near Field Pressure Signatures to Wind Tunnel Data

To obtain information on the ground signature of these two configurations, the method and computer code of Thomas (Ref. 6) was used to extrapolate both near field wind tunnel model data and computations. The computer code of Thomas uses the waveform parameter method for sonic boom extrapolation which is shown to be equivalent to the F-function method and is based on the same fundamental concepts from geometric acoustics and isentropic wave theory. It is ideal for this application because it accepts as input any height pressure signature data below or to the side of the aircraft and accounts for atmospheric effects. Figure 14 shows the extrapolated ground signatures for both the computed and wind tunnel data for the Mach 2 configuration flying at 55,000 feet. A reflection factor of 1.9 was used at the ground in the Thomas code. The wind tunnel data measured at distances of one half and one body length and computed results at $h/\ell = 0.50$, 1.0 and 3.0 were extrapolated to see the effect of nonlinearities and three-dimensional effects on the ground signatures. The initial overpressure from the extrapolated wind tunnel data (Fig. 14b) varies between 1.1 and 1.2 lbs/ft^2. The extrapolated computed signatures shown in Fig. 14a show a variation in the initial overpressure of 1.15 to 1.25 in good agreement with the wind tunnel data. The computed signatures extrapolated from $h/\ell = 0.50$ and 1.0 correspond to the shorter sting and slightly higher resolution. These signatures show a secondary shock at about 300 feet aft of the initial overpressure. The extrapolated signature from $h/\ell = 3$ does not have this secondary shock but shows a steeper compression prior to 200 feet. Figure 14c shows two extrapolated computations from $h/\ell = 1.0$ and 3.0 compared to the wind tunnel data extrapolated from $h/\ell = 1.0$. Overall good agreement with the wind tunnel data is achieved. The secondary shocks and the strengths of the tail shock is not predicted well.

Figure 15 shows both the wind tunnel data and computed results extrapolated to the ground using the method of Thomas for the Mach 3 configuration flying at 65,000 feet. The wind tunnel data at both measured distances below the aircraft are extrapolated and are shown in Fig. 15b. At $h/\ell = .7$, the data extrapolation indicates an initial bow shock rise of about 1.8 lbs/ft^2 and a secondary shock rise to 2.4 lbs/ft^2. The extrapolated ground signature from data at $h/\ell = 1.0$ indicates some coalescence with an initial shock rise to about 1.6 and a secondary shock rise to about 1.8 lbs/ft^2. Hence, for the Mach 3 configuration, the extrapolated ground signature is sensitive to the distance below the aircraft where data has been taken. Figure 15a shows the ground signatures extrapolated from the computed results at several locations below the aircraft corresponding to $h/\ell = 0.5$, 1.0 and 3.0. The computed results at $h/\ell = 0.5$ and 1.0 come from the model with the shorter sting and slightly higher resolution. The $h/\ell = 3.0$ extrapolation was for the model with the long sting. The initial shock rise is in agreement for all these extrapolated signatures. A small secondary shock occurs near the end of the aircraft or at about 300 feet in the signature. This shock is only predicted for the highly resolution signatures. The tail shock occurs further aft and grows in strength as the distance for extrapolation increases. Figure 15c also shows a comparison of the extrapolated signatures from wind tunnel data and computations at $h/\ell = 1.0$. The comparison is in good agreement except that the wind tunnel data shows a stronger secondary shock in a different location than the computation. Both indicate an initial shock rise of about 1.6 lbs/ft^2. The wind tunnel data shows a secondary rise to about 1.8 lbs/ft^2.

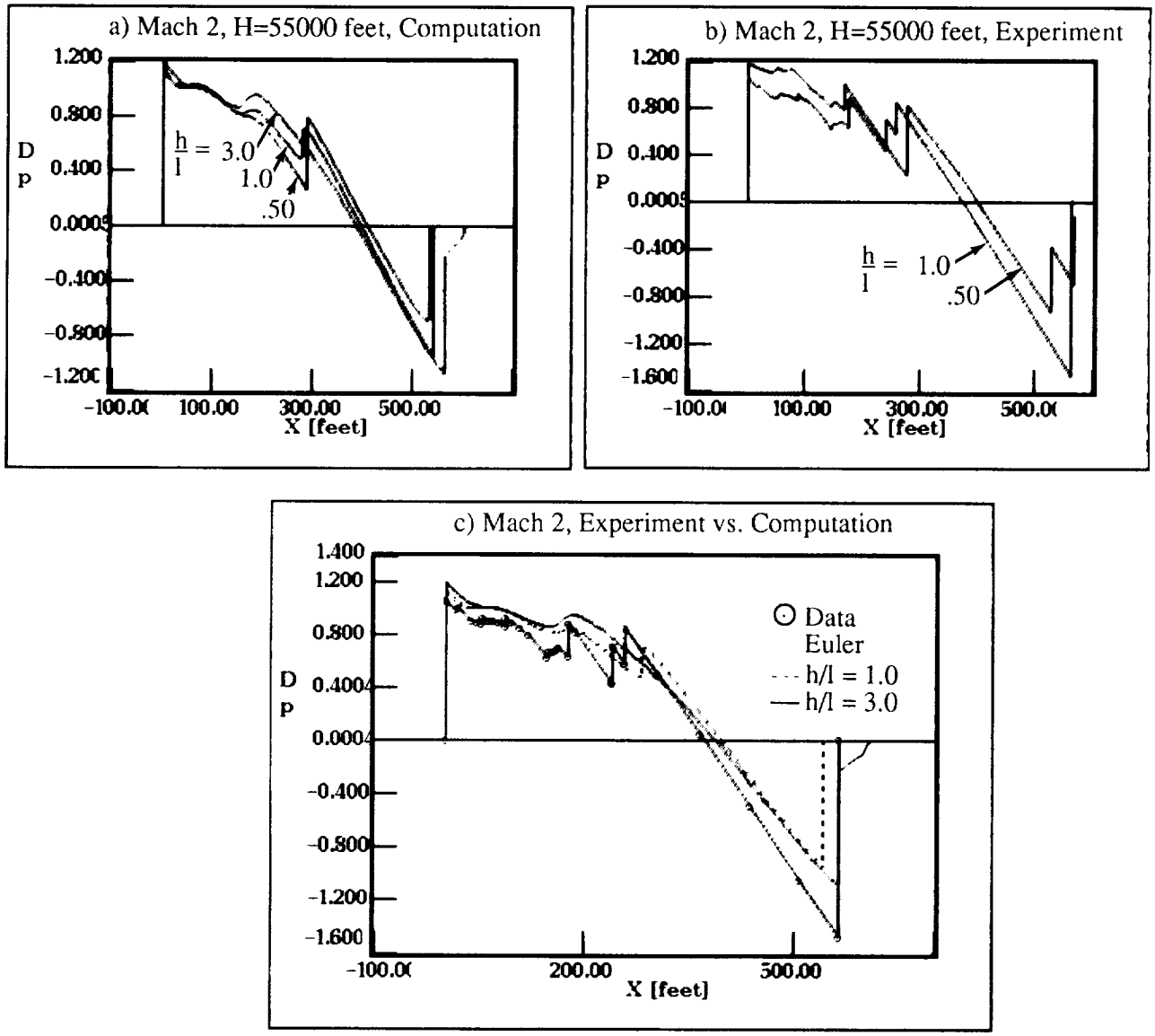

Figure 14 Comparison of Extrapolated Ground Signatures to Extrapolated Wind Tunnel Data for the Mach 2 Configuration

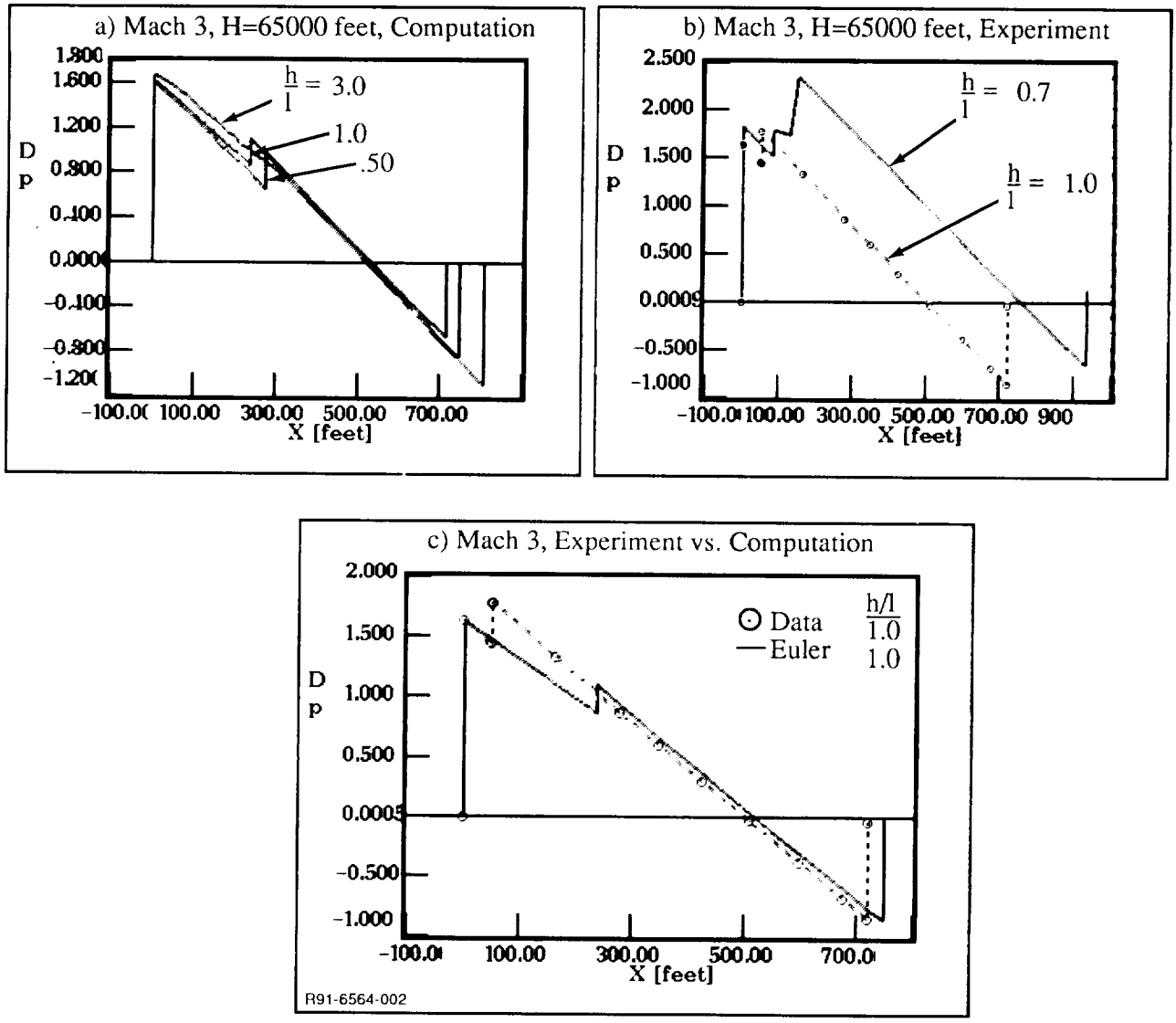

Figure 15 Comparison of Extrapolated Ground Signatures to Extrapolated Wind Tunnel Data for the Mach 3 Configuration

Figure 16 shows the three-dimensional computed pressure footprint generated by the Mach 2 configuration at $h/\ell = 1.0$ below the aircraft. The computed results are from the model using the slightly longer sting. The pressure footprint is plotted laterally out to two aircraft lengths. Plotted to the left of the three dimensional footprint are pressure signatures at constant lateral distances or azimuthal angles from the centerline of the aircraft. At the first signature off the axis ($\varphi = 14°$), the effect of the strong wing crank shock begins to become prominent in the form of a second shock. In the third ($\varphi = 26.6°$) and fourth ($\varphi = 36.9°$) signatures, the first overpressure begins to diminish and the second overpressure due to the wing crank shock increases to an overpressure value greater than the value of the bow shock overpressure at the centerline. In addition, the large expansion due to the wing tips also becomes prominent on the off centerline signatures.

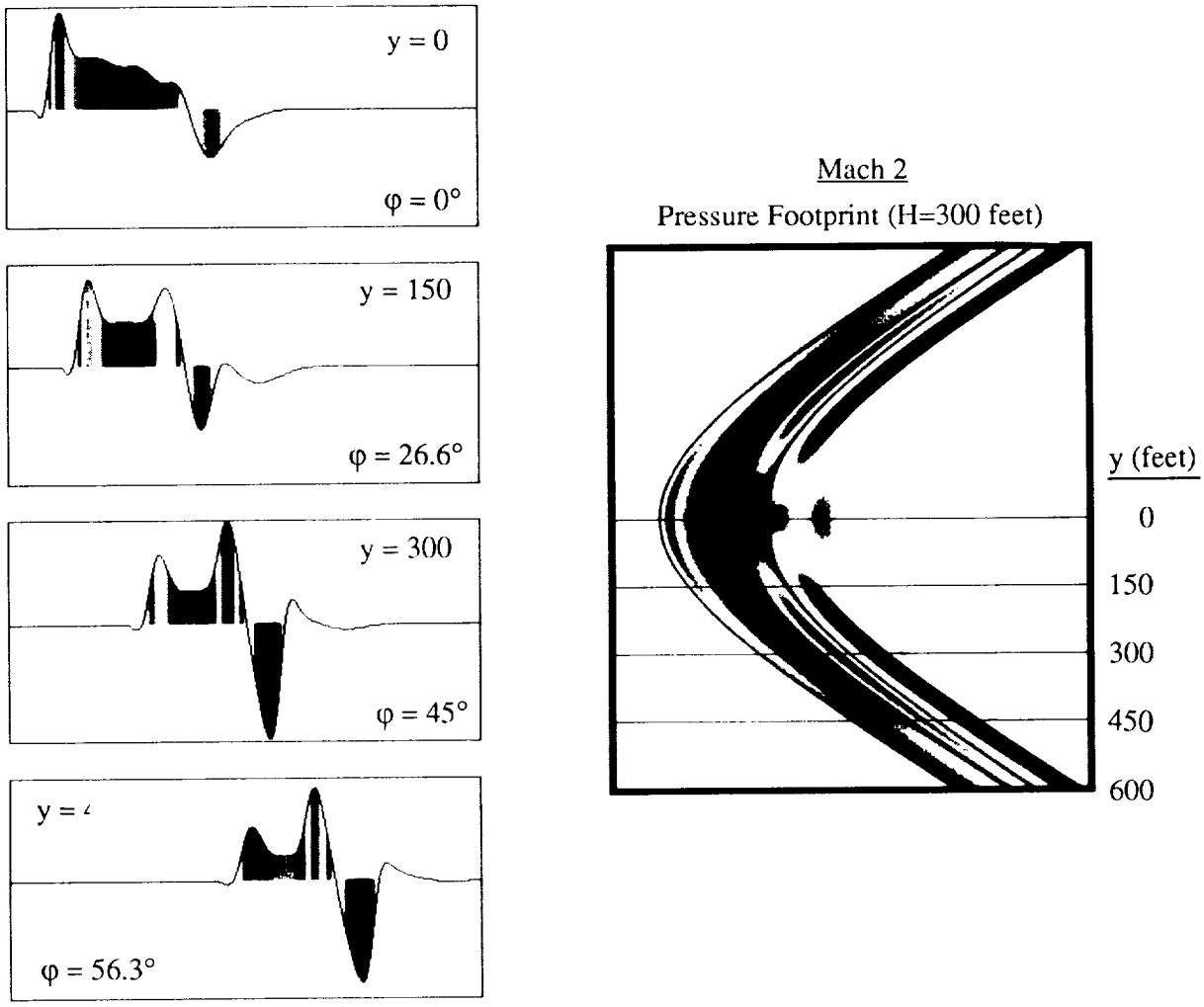

Figure 16 Three-Dimensional Pressure Footprint of the Mach 2 Aircraft at $h/\ell = 1.0$

Figure 17 shows the same type of plot for the Mach 2 configuration except that the three-dimensional footprint corresponds to an $h/\ell = 3.0$ below the aircraft. In this figure, the footprint is plotted out to a lateral distance of three aircraft lengths. A similar behavior of the off axis pressure signatures is indicated. The signature at $\varphi = 26.6°$ are plotted in both Figure 16 and 17 and occur along the same azimuthal ray and look very similar. Hence, the three-dimensional or off centerline behavior of the sonic boom footprint does not seem to vary significantly from an $h/\ell = 1.0$ to an $h/\ell = 3.0$ below the aircraft.

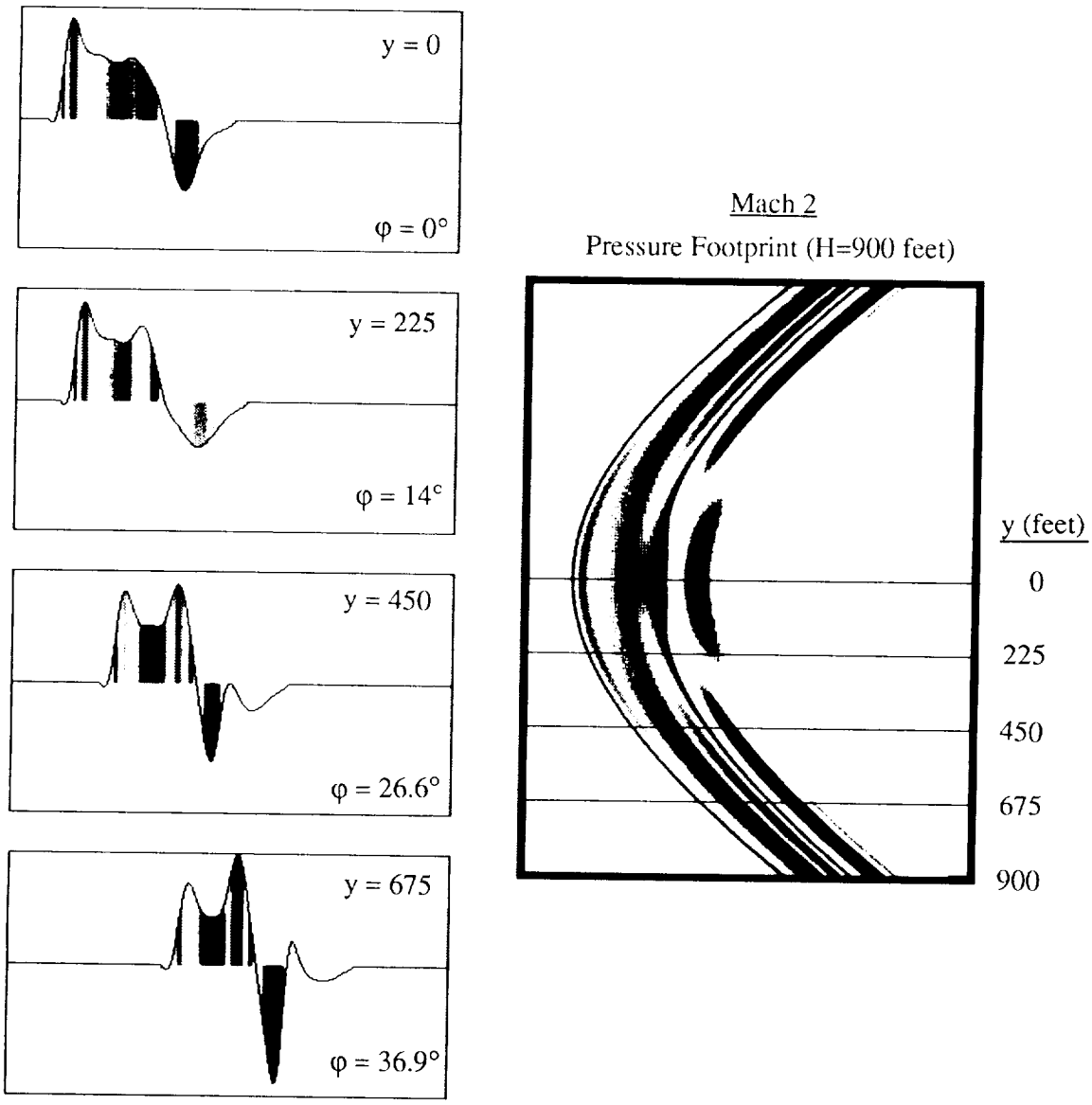

Figure 17 Three-Dimensional Pressure Footprint of the Mach 2 Aircraft at $h/\ell = 3.0$

To determine the three-dimensional behavior of the ground sonic boom for the Mach 2 configuration footprint, the signatures of Figures 16 and 17 were input to the Thomas sonic boom extrapolation code. Figure 18 shows the resulting ground signatures for the Mach 2 configuration flying at an altitude of 55,000 feet. $\varphi = 0°$ corresponds to the flight path ground axis. If two azimuthal angles were the same from Figures 16 and 17, both signatures were extrapolated. At 5.72 miles from flight path centerline, the initial bow shock rise decays slightly but a second stronger overpressure occurs due to the wing crank shock at about 1.45 lbs/ft^2. Further off the centerline at 8.73 miles, the second overpressure rises to almost 1.5 lbs/sq ft. At 12.44 miles from flight path centerline, the second overpressure begins to diminish. The Thomas extrapolation method also indicates that these two shocks begin to coalesce into a single larger initial boom in comparison to the signature along the centerline. The three-dimensional results also indicate that boom overpressures up to 25% greater in magnitude can be felt to the side of the aircraft flight path axis due to the aircraft's supersonic leading edge wing crank.

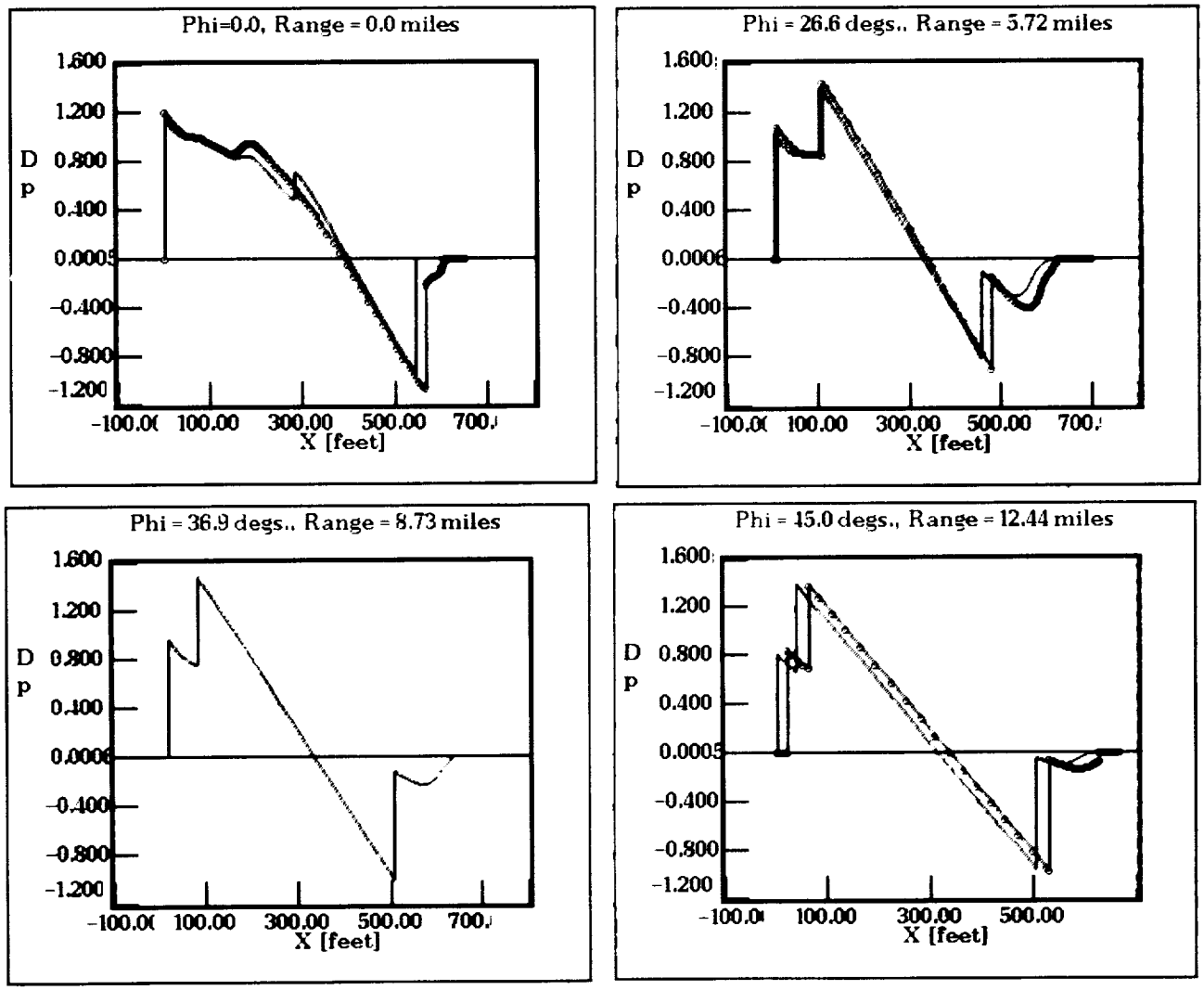

Figure 18 Off Flight Path Axis Ground Extrapolations for the Mach 2 Configuration

Figure 19 shows the three-dimensional footprint computed for the Mach 3 configuration at h/ℓ = 1.0 below the aircraft. A similar pattern of behavior occurs for the Mach 3 configuration as was indicated for the Mach 2 model. A strong second shock occurs off the centerline due to the wing crank shock whose magnitude is equal or slightly greater than the centerline overpressure.

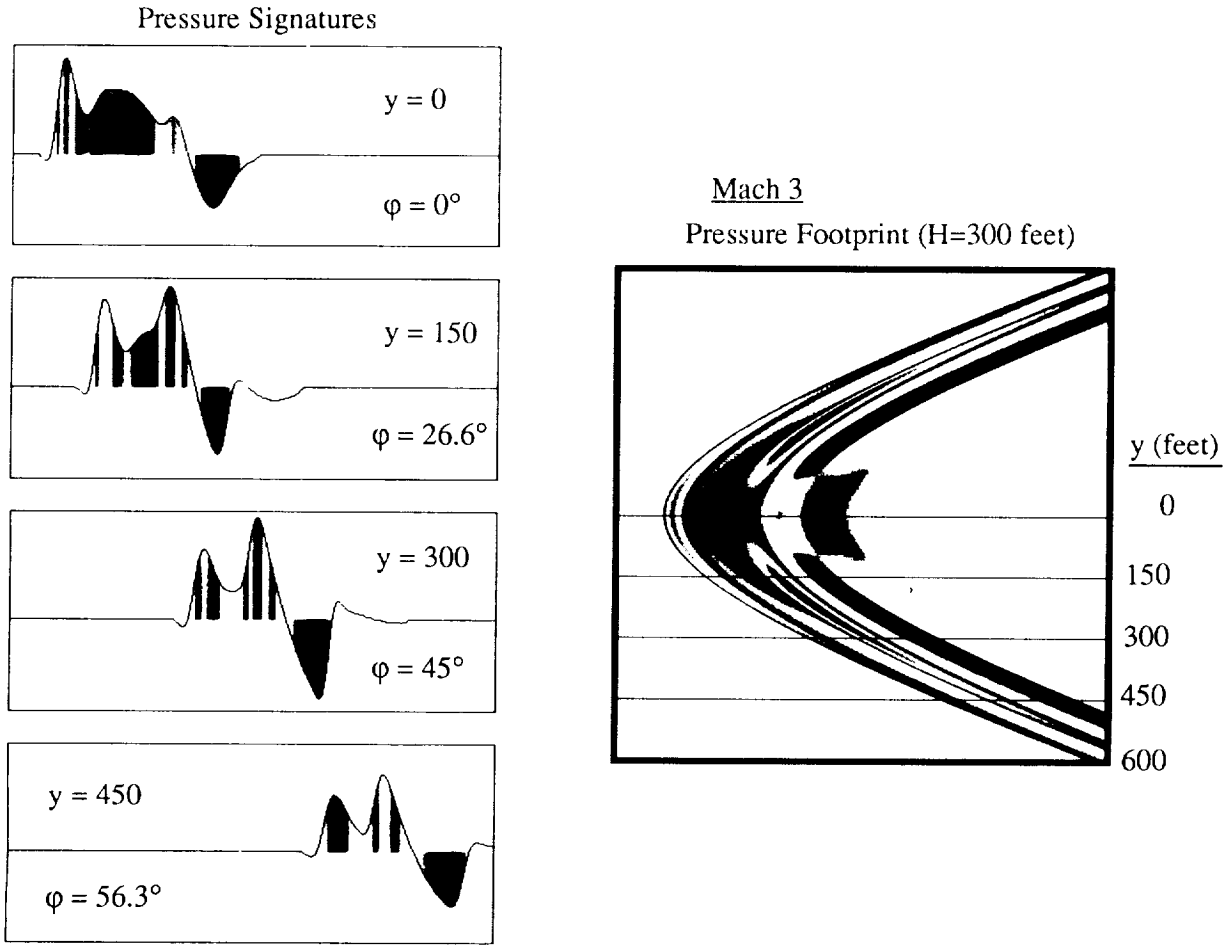

Figure 19 Three-Dimensional Pressure Footprint of the Mach 3 Aircraft at h/ℓ = 1.0

Figure 20 shows a similar set of plots for the three-dimensional pressure footprint of the Mach 3 configuration but at $h/\ell = 3.0$ below the aircraft. This footprint extends to three aircraft lengths off the axis. Comparing the signatures in Figures 19 and 20 at $\varphi = 26.6°$, the second overpressure is rising well above the initial bow shock rise.

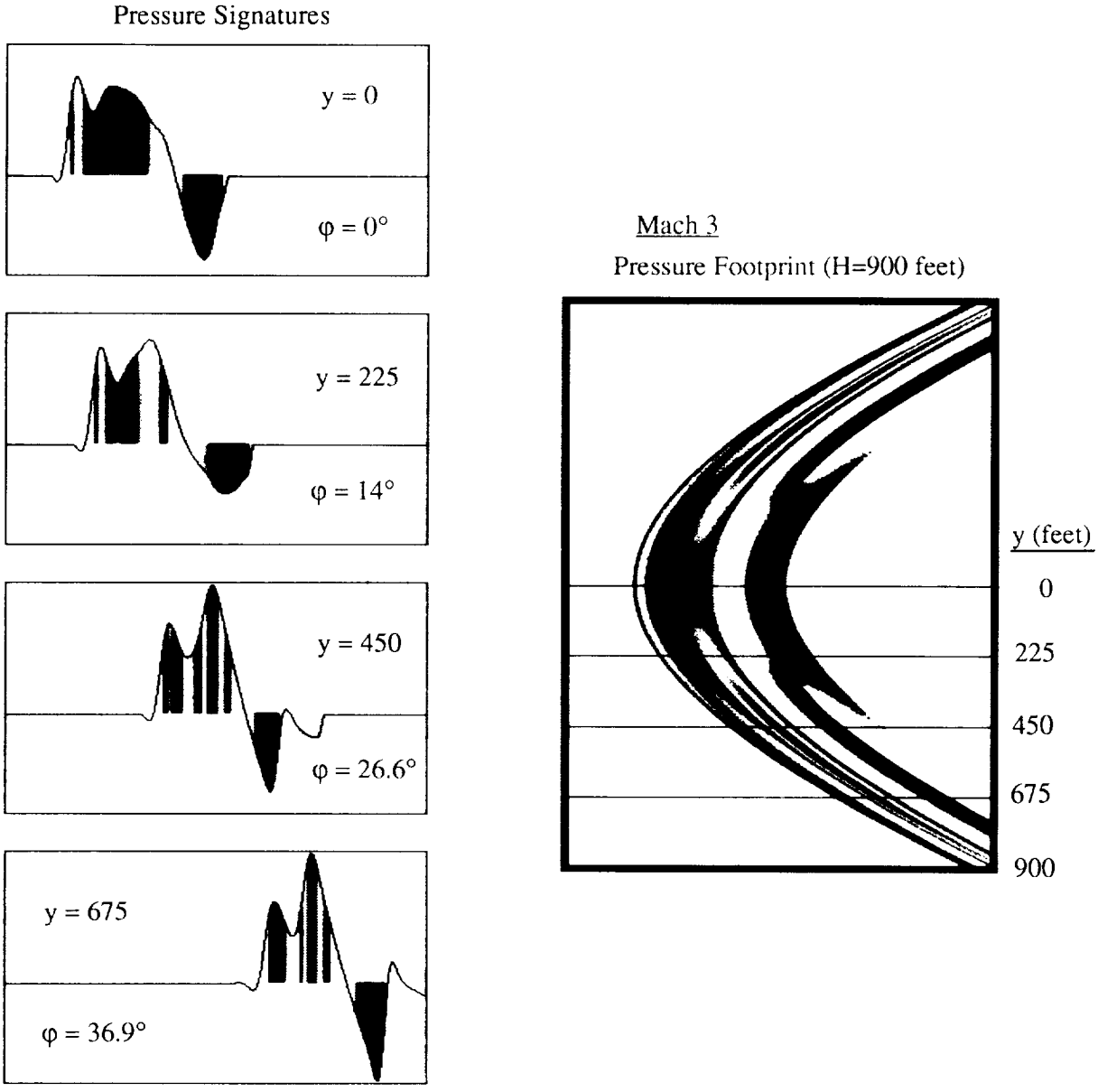

Figure 20 Three-Dimensional Pressure Footprint of the Mach 3 Aircraft at $h/\ell = 3.0$

Figure 21 shows the corresponding ground signatures extrapolated using the Thomas code for the Mach 3 configuration flying at 65,000 feet. In contrast to the ground behavior of the Mach 2 configuration, the Thomas code essentially predicts the coalescence of the bow shock with the second overpressure into a typical N wave. The off aircraft axis signatures only show a 10% rise in comparison to the centerline. The strength of the signature or boom remains relatively constant due to the second shock up to 10 miles from the flight path centerline, at which point, the boom begins to decay due to the long ray path to reach the ground.

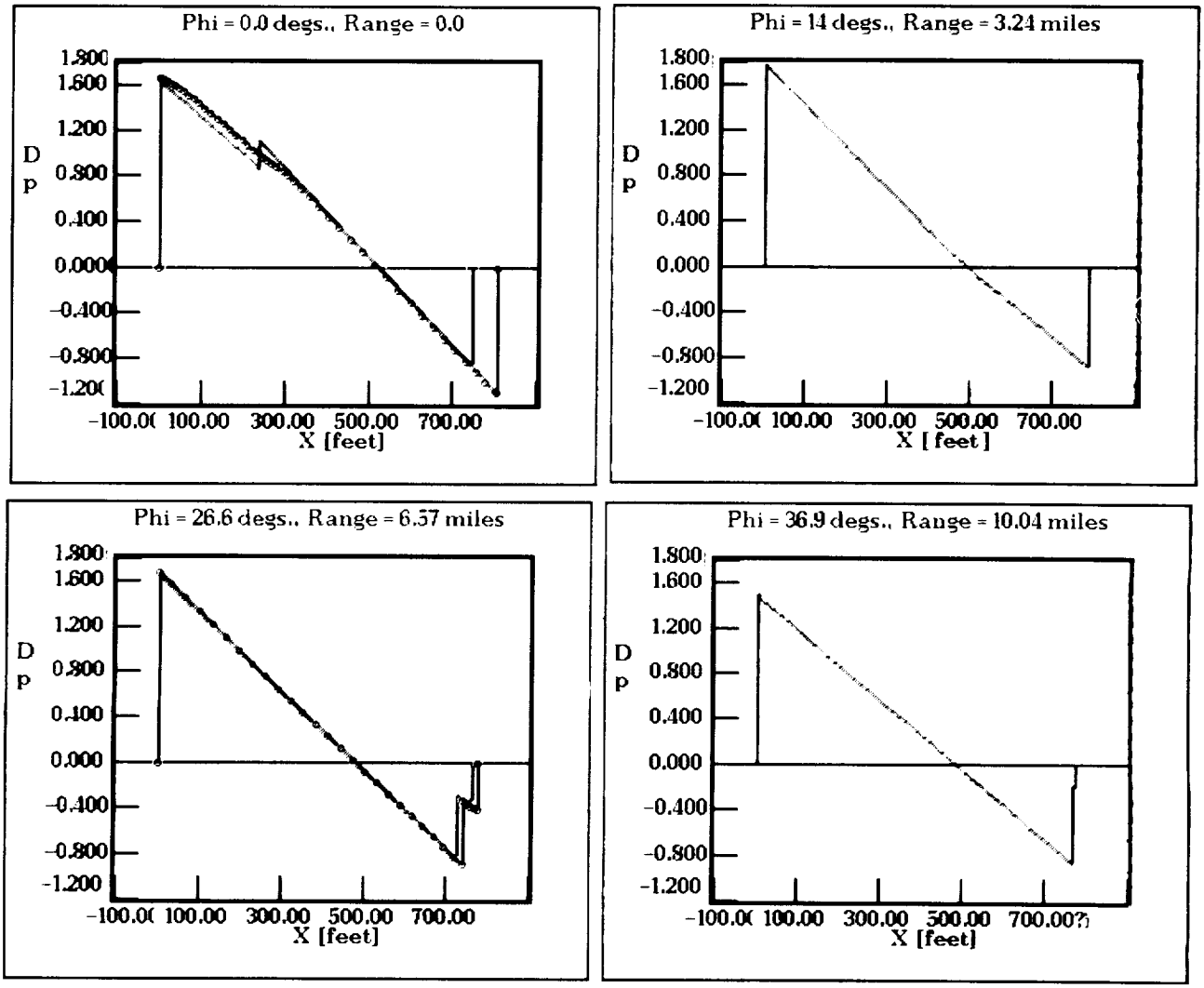

Figure 21 Off Flight Path Axis Ground Extrapolations for the Mach 3 Configuration

REFERENCES

1. Mack, R.J. and Darden, C.M., private communication, April, 1991, data to be published.

2. Jameson, A., "A Vertex Based Multigrid Algorithm for Three-Dimensional Compressible Flow Calculations," ASME Symposium on Numerical Methods for Compressible Flow, Anaheim, CA, Dec. 1986.

3. Siclari, M.J., "Hybrid Finite Volume Approach to Euler Solutions for Supersonic Flows," AIAA J., Vol. 28, No. 1, Jan. 1990, pp. 66-74.

4. Siclari, J., "Three-Dimensional Hybrid Finite Volume Solutions to the Euler Equations for Supersonic/Hypersonic Aircraft," AIAA Paper No. 89-0281, presented at the 27th Aerospace Sciences Meeting, Reno, NV, Jan. 1989.

5. Siclari, M and Darden, C., "An Euler Code Prediction of Near to Mid-Field Sonic Boom Pressure Signatures," AIAA Paper No. 90-4000, presented at the AIAA 13th Aeroacoustics Conference, Tallahassee, FL, Oct., 1990.

6. Thomas, C.L., "Extrapolation of Sonic Boom Pressure Signatures by the Waveform Parameter Method," NASA TN D-6832, June 1972.